

Supporting Information

An Insight on the Effect of Azobenzene Functionalities Studied in UiO-66 Framework for Low Energy CO₂ capture and CO₂/N₂ Membrane Separation

Nicholaus Prasetya, and Bradley P. Ladewig*

MOF Characterizations

The ligand structure used in this study is shown in Figure S 1.

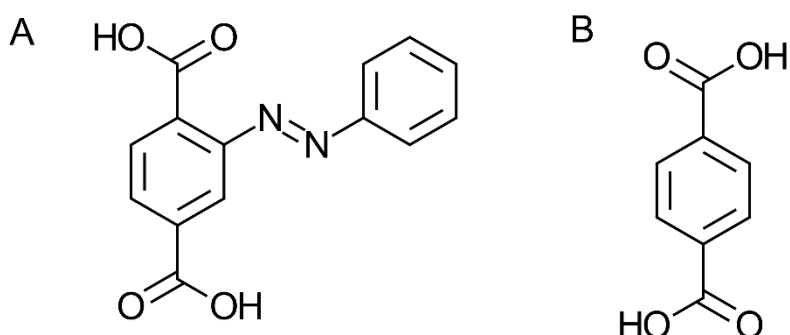


Figure S 1. Chemical structure of L1 (A) and L2 (B) used in this study

The structural building unit of the MOFs in Figure 1 in the main manuscript is created by using CrystalMaker software. The building unit is considered hypothetical and the amount of azobenzene and terephthalate linker in the picture is based on the calculation described below

The $^1\text{H-NMR}$ spectrum of the MOF synthesized using mixed ligand are shown in Figure S 3, Figure S 2 and Figure S 4. The main objective for $^1\text{H-NMR}$ characterization is to estimate the ratio between terephthalate and azobenzene ligand in the framework. This process is accomplished as follow. First, the singlet peak at 7.6 ppm was integrated since this peak belongs to the terephthalate ligand (L2). The integrated value was then normalized to 4 as terephthalate ligand has 4 protons. Afterwards, the integration was proceeded for the rest of the peaks that belong to the azobenzene ligand followed by summation for all of the integrated peaks. It should be noted that differ from terephthalate, 1 azobenzene ligand has 8 protons. This ratio was then used to calculate the actual ratio between L1 and L2 in the framework. Therefore, for example, if the framework is assumed to contain equal amount of L1 and L2, the ratio of the integrated peaks from azobenzene and terephthalate should be 8:4. Finally, the amount of the each ligand in the framework was then calculated by assuming that the Azo(X)-UiO-66 is linked by 12 ligands as in UiO-66. The final calculation of the ligand ratio found in the mixed ligand Azo(X)-UiO-66 is given in Table S 1.

Table S 1. Calculation of L1 and L2 in the MOF framework from $^1\text{H-NMR}$ data

MOF	Integrated L1	Integrated L2	Actual L1:L2 (approx.)	Amount of L1 in the framework	Amount of L2 in the framework
Azo(16.7)-UiO-66	1.59	4	1:5	2	10
Azo(33.3)-UiO-66	4.15	4	1:2	4	8
Azo(66.7)-UiO-66	16.08	4	2:1	8	4

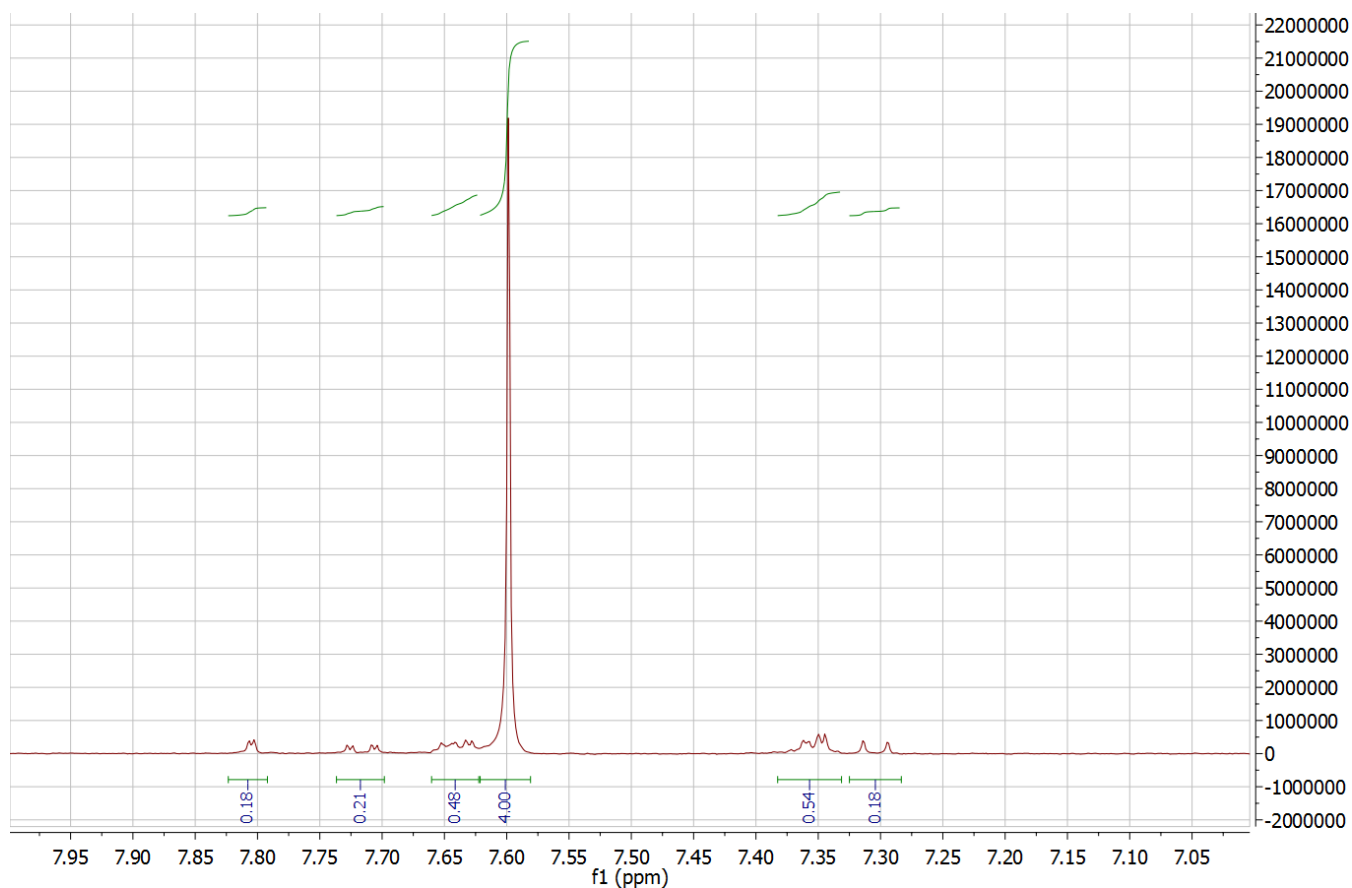


Figure S 2. $^1\text{H-NMR}$ spectrum of digested Azo(16.7)-UiO-66

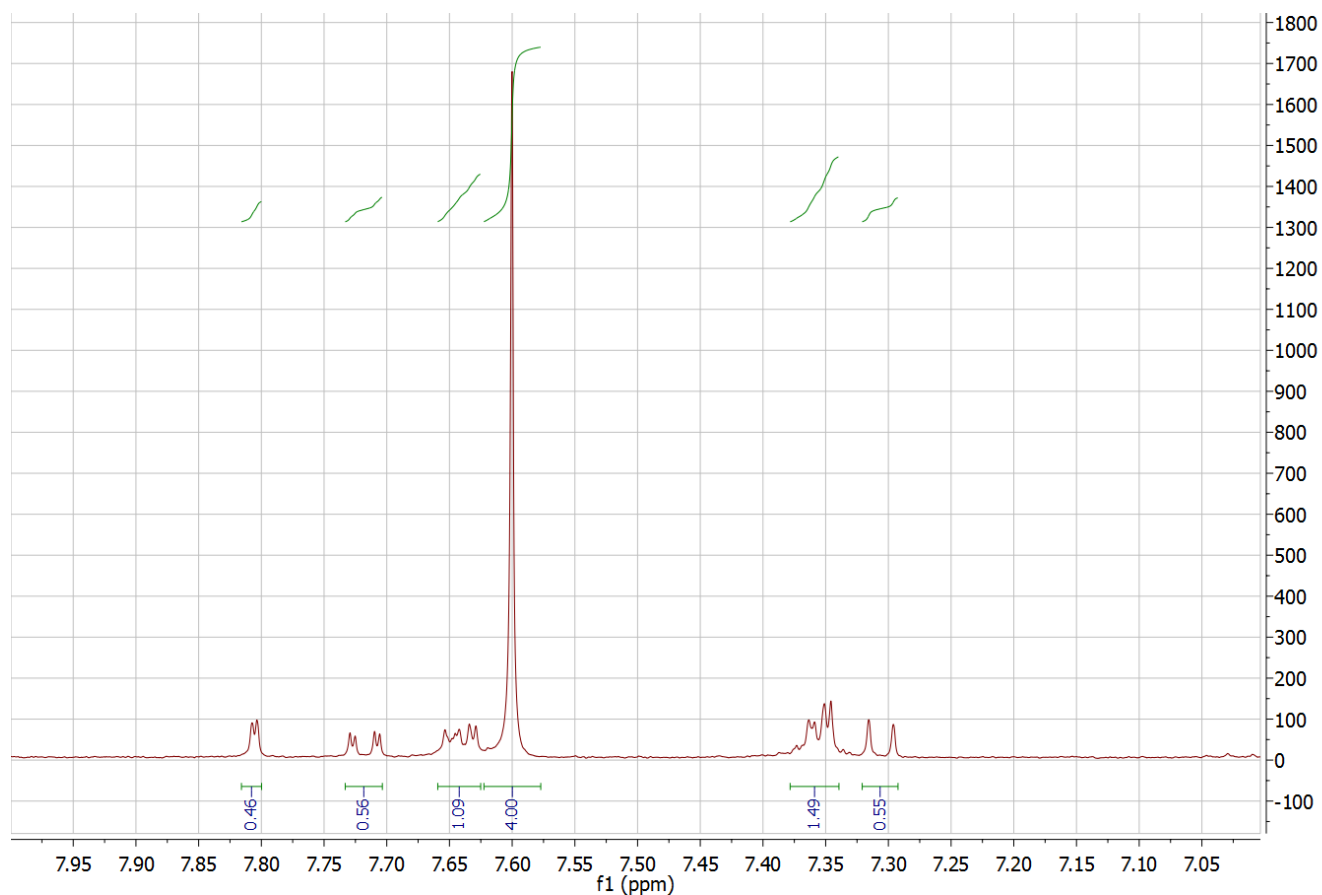


Figure S 3. $^1\text{H-NMR}$ spectrum of digested Azo(33.3)-UiO-66

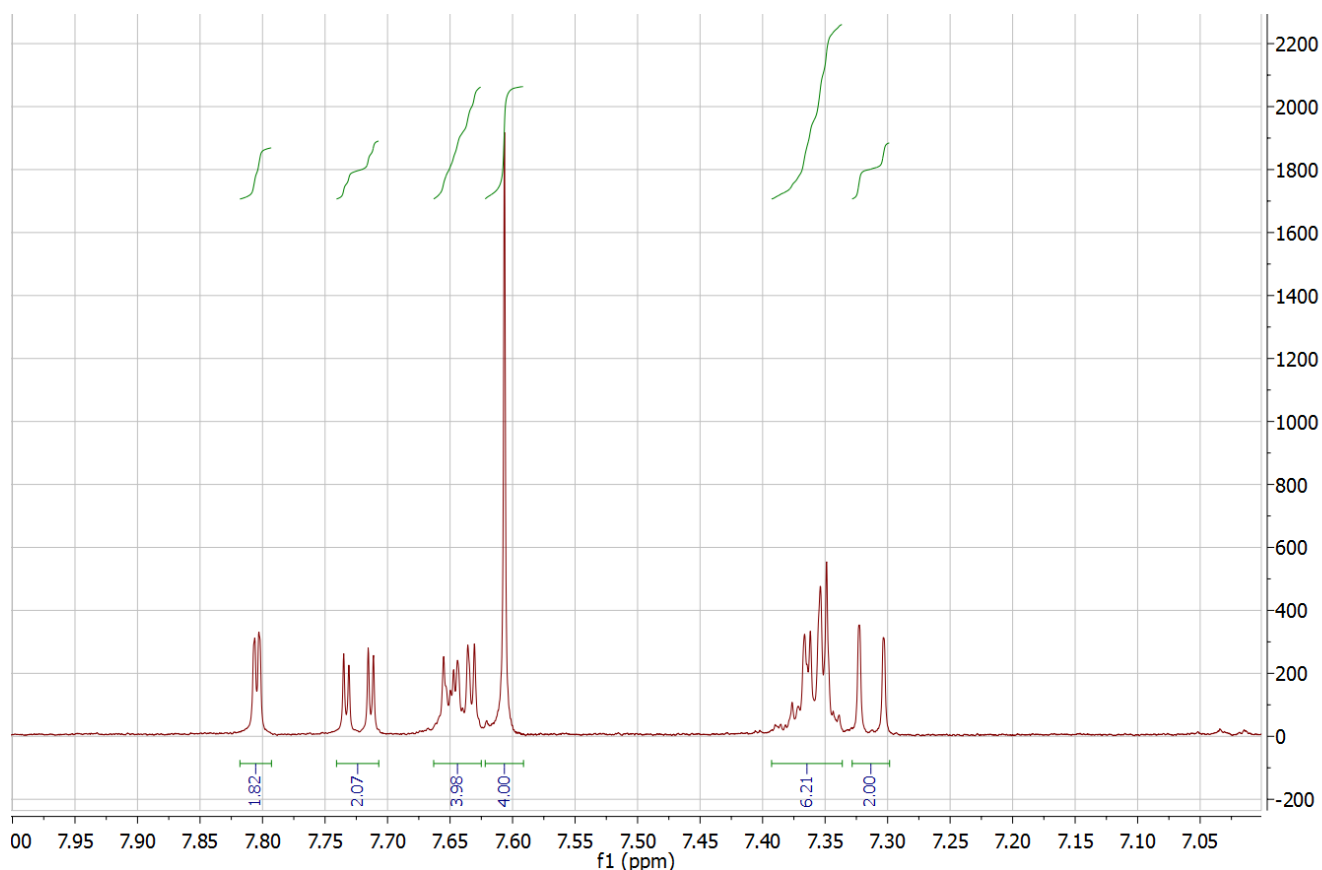


Figure S 4. ^1H -NMR spectrum of digested Azo(66.7)-UiO-66

The UV Vis spectra of the digested MOFs is given in Figure S 5. As can be seen, an increase in azobenzene functionality in MOF framework also resulted in higher absorbance intensity both at 322 and 423 nm. Meanwhile, UiO-66 did not give any absorbance across the observed wavelength.

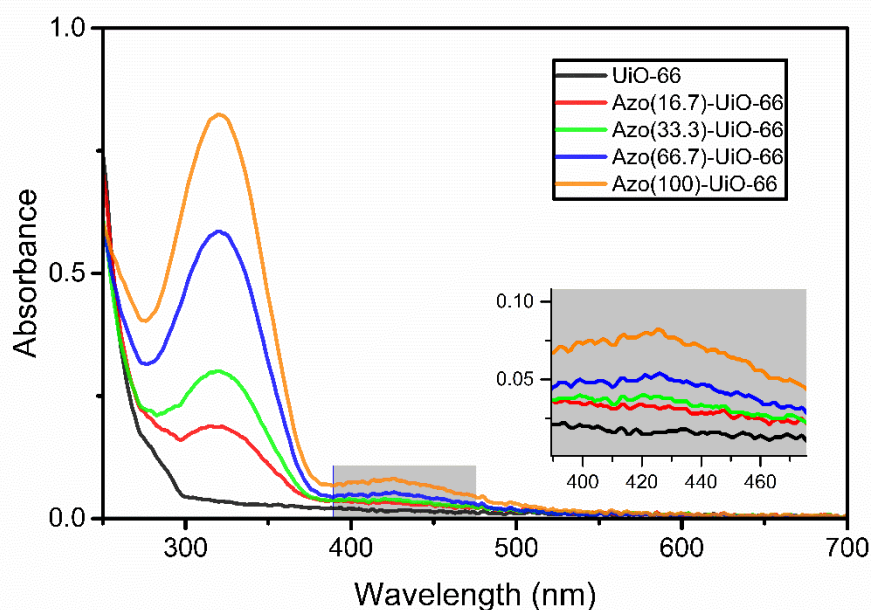


Figure S 5. UV-Vis spectra of the digested UiO-66 and Azo(X)-UiO-66

A combination of UV-Vis spectra and ^1H -NMR data could then be used to estimate the azobenzene concentration inside the framework as previously suggested in NH_2 -UiO-66.^[1] The same method is then employed here with the calibration curve and the result is given in Figure S 6 and Table S 2, respectively.

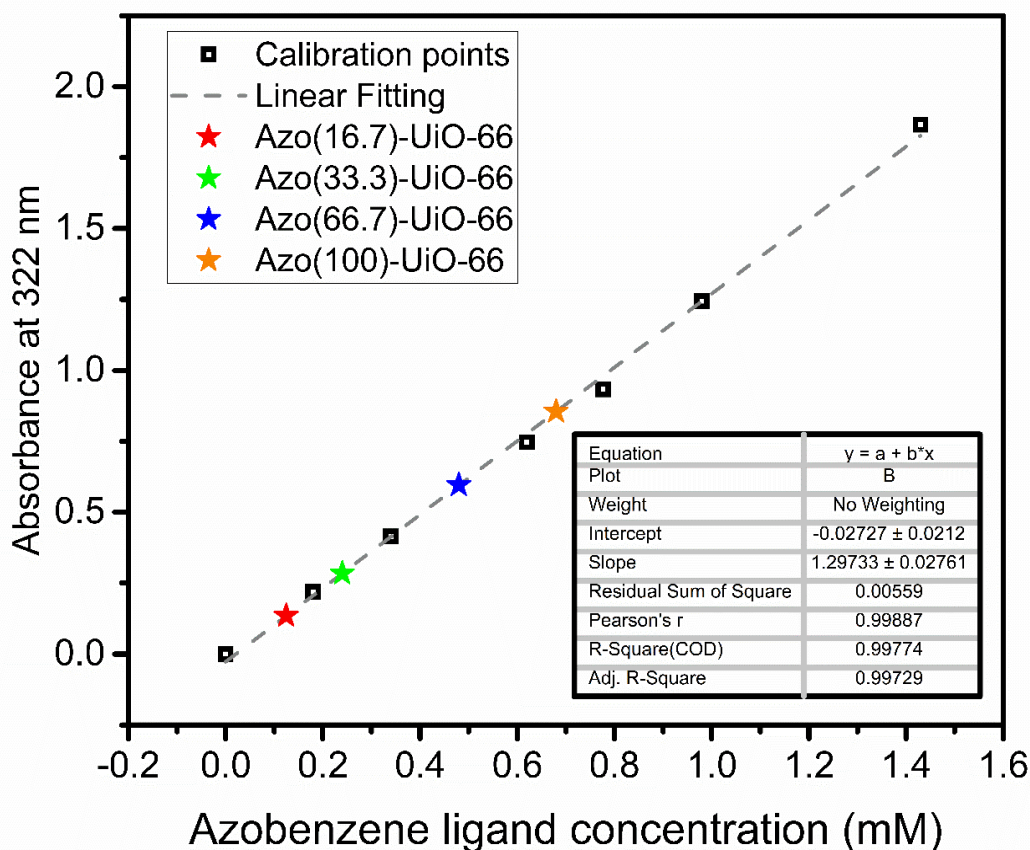


Figure S 6. UV-Vis spectra calibration curve and the points of digested Azo(X)-UiO-66

Table S 2. Calculation of azo ligand concentration in the MOF framework through UV-Vis spectra approach

MOF	Azo ligand(L1) ^a	BDC ligand (L2) ^a	MW ^b	Sample mass (mg) ^c	Sample volume (mL) ^c	Calculated [azo] (mM) ^d	Experiment [azo] (mM) ^e
UiO-66	0	12	2647.32	0.87	4	0	0
Azo(16.7)-UiO-66	2	10	2855.32	0.85	4	0.149	0.141
Azo(33.3)-UiO-66	4	8	3063.32	0.94	4.5	0.271	0.289
Azo(66.7)-UiO-66	8	4	3479.32	0.81	3.6	0.517	0.599
Azo(100)-UiO-66	12	0	3895.32	1.14	4.8	0.732	0.857

a the value of azo ligand (L1) and bdc ligand (L2) in the mixed ligand MOFs were approximated from ¹H-NMR data. This value will also be used to calculate the ideal molecular weight (MW) of the MOFs

b It is firstly assumed that all the MOFs are connected with 12 ligands. The molecular weight (MW) value is based on the building unit of the UiO-66, namely $Zr_6(O)_4(OH)_4(azo)_x(bdc)_y$ where x and y represents the amount of azo and bdc ligand in the framework based on the ¹H-NMR data.

c the mass of the samples and volume of NaOH solution prepared to obtain UV-Vis spectra of the samples

d this is calculated based on the formula $calculated [azo] = (amount\ of\ azo \times MW\ azo) / (MW\ MOF) \times (sample\ mass) / (sample\ volume)$

e this is obtained by interpolating the absorbance at 322 nm of the samples in the calibration curve

It could be seen that both calculated and experiment azobenzene concentration in the framework are quite close to each other. This means that the value calculated from the assumed $^1\text{H-NMR}$ data is quite accurate to predict the constituents of the ligand in the frameworks.

The FTIR spectra of all the MOFs are given in Figure S 7. As can be seen, as the azobenzene concentration in the MOF framework was increased, the relative transmittance intensity of the peaks at 1370 cm^{-1} and 770 cm^{-1} also increased. These peaks correspond to the azobenzene vibration as they did not appear in UiO-66 and barely observed in Azo(16.7)-UiO-66.

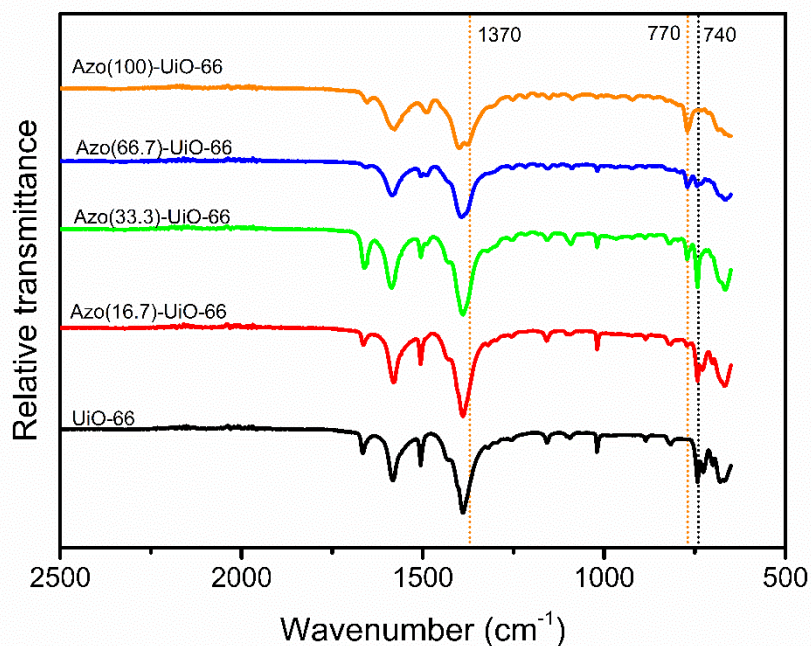


Figure S 7. FTIR spectra of UiO-66 and Azo(X)-UiO-66

The thermal stability of all the MOFs are given in Figure S 8. As can be seen, there are two thermal decomposition regions. The mass loss below 100°C is due to the moisture loss from the MOF surface. It could be seen that azobenzene functionality might impart hydrophobic property of towards the MOF as evidenced from higher mass loss in this region in MOFs with less azobenzene functionality and UiO-66. However, as the azobenzene functionality was increased, the MOF was also more prone to suffer thermal decomposition at

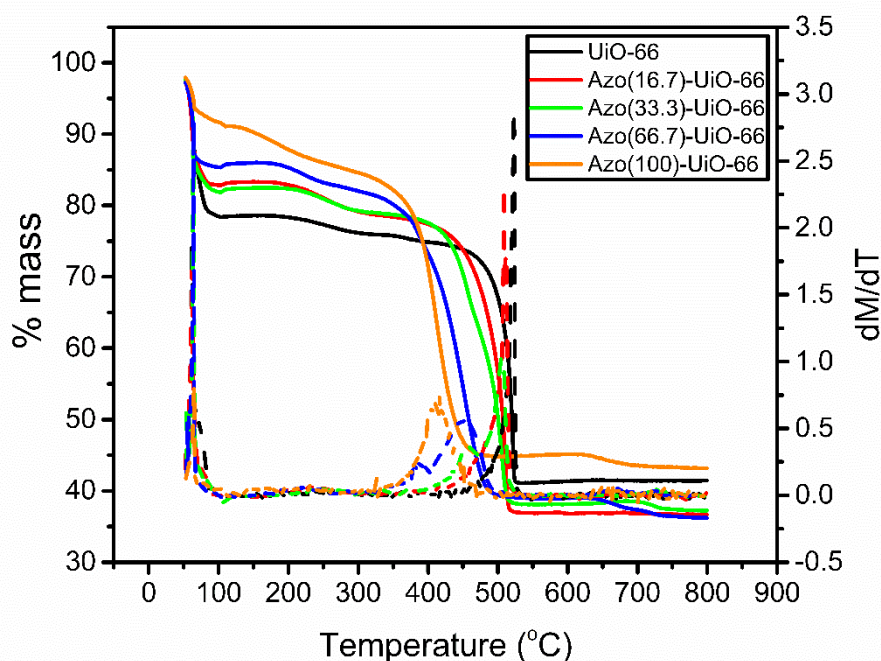


Figure S 8. TGA data of UiO-66 and Azo(X)-UiO-66

lower temperature. As can be seen, the decomposition of Azo(100)-UiO-66 started at about 350°C while the UiO-66 was stable up to 450°C. This could be caused by less crystalline structure at higher azobenzene concentration as also observed in PXRD pattern of the MOFs.

It has been previously reported that both UiO-66^[2] and Azo(100)-UiO-66^[3] are stable after water immersion. Therefore, water stability for the mixed-ligand Azo(X)-UiO-66 was also investigated by checking their PXRD diffraction pattern and the result is given in Figure S 9. After immersed in water for 24 hours, it could be seen that all the mixed ligand Azo(X)-UiO-66 could maintain their crystalline structure indicating their structural robustness. Therefore, the presence of mixed ligands in the framework does not alter the UiO-66 framework stability under water.

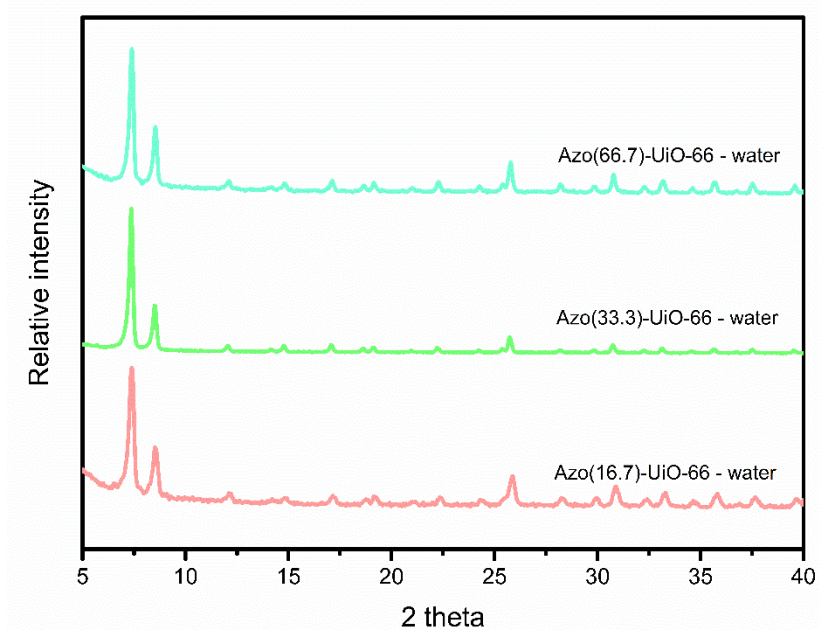


Figure S 9. PXRD diffraction pattern of Azo(16.7)-, Azo(33.3)-, and Azo(66.7)-UiO-66 after 1 day water immersion

Lastly, the synthesized MOFs in this study were also characterized through SEM and the result is given in *Figure S 10*. As can be seen, the all the particles synthesized in this study were in the nanometer range. Specifically, they were in the range of 100-200 nm.

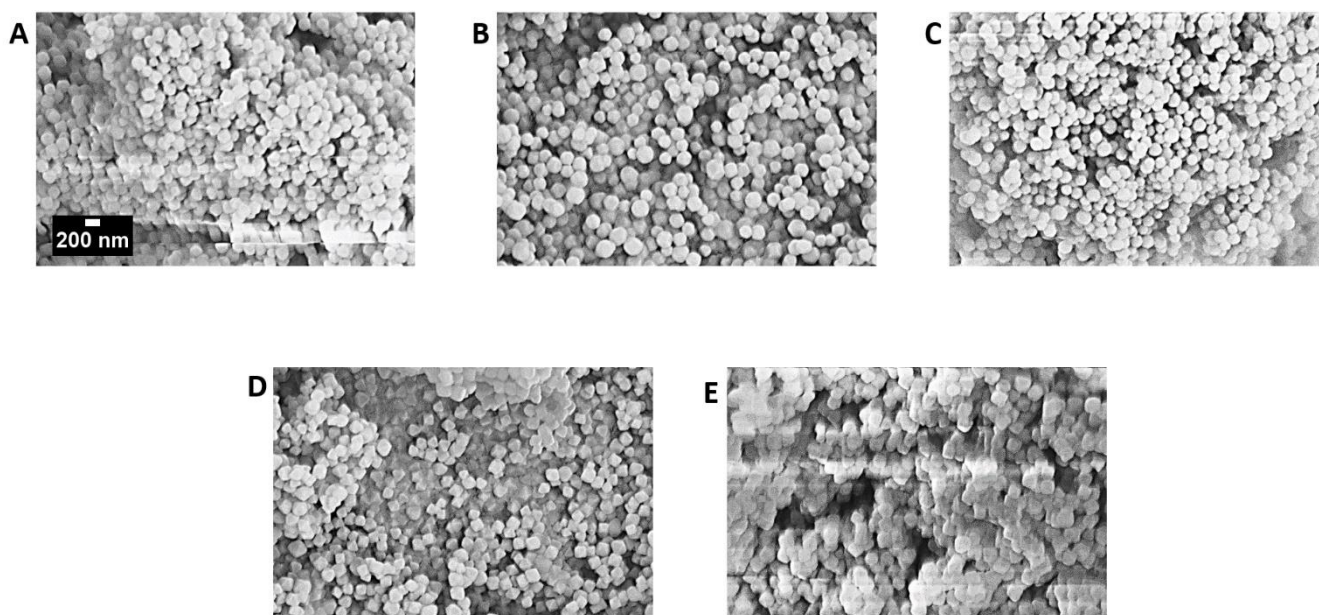


Figure S 10. SEM micrograph of UiO-66 (A), Azo(16.7)-UiO-66 (B), Azo(33.3)-UiO-66 (C), Azo(66.7)-UiO-66 (D) and Azo(100)-UiO-66 (E) synthesized in this study

MOF adsorption properties

The pore width distribution of the MOFs were given in Figure S 11. As can be seen, a decreasing trend in dV/dW value could be observed as the azobenzene concentration in the MOF pore was increased. Since this value is calculated based on the pore volume of the MOFs, this also highlights the significance reduction in MOF pore volume at higher azobenzene concentration in the MOF pores. In addition, it could also be seen that higher azobenzene loading leads to the pore width expansion as evidenced from the broadening of the pore with peak, in particular for the Azo(66.7)- and Azo(100)-UiO-66. This could be caused by the MOF frameworks trying to accommodate more azobenzene functionalities to fit inside their pores.

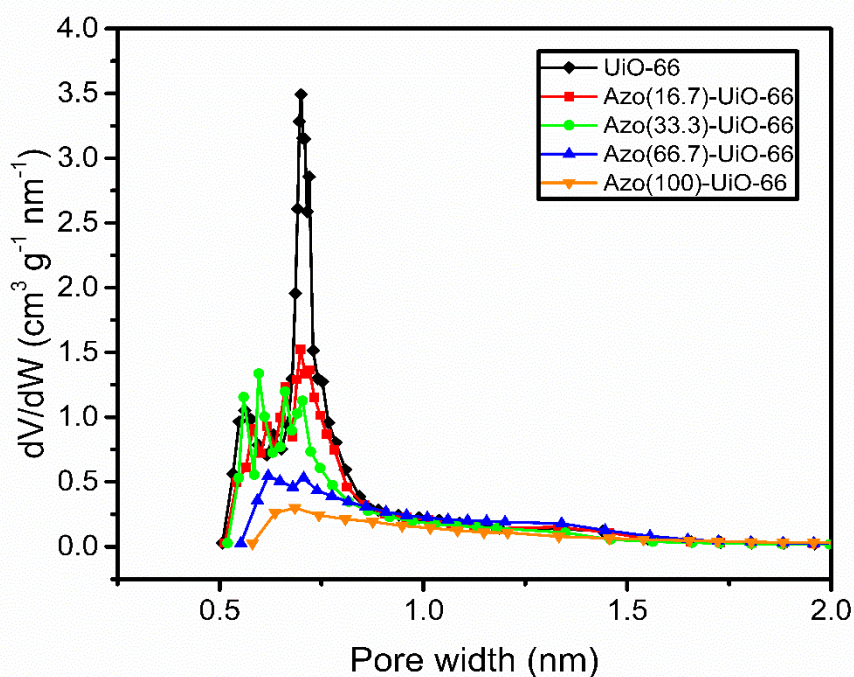


Figure S 11. Pore width distribution of UiO-66 and Azo(X)-UiO-66

The CO₂ adsorption of all MOFs at 273 K and the dynamic CO₂ photoswitching at 273 K are given in Figure S 12 and Figure S 13, respectively, As can be seen in Figure S 12, the behavior of CO₂ adsorption at 273 K is similar with the CO₂ uptake at 298 K. Both Azo(16.7) and Azo(33.3) were found to have slightly higher CO₂ uptake compared with UiO-66 which might be caused by higher affinity of CO₂ and the framework. Meanwhile, the CO₂ uptake for Azo(66.7) and Azo(100)-UiO-66 had the lowest CO₂ uptake as also observed in the CO₂ uptake at 298 K showing the negative impact coming from the steric effect of the azobenzene functionality.

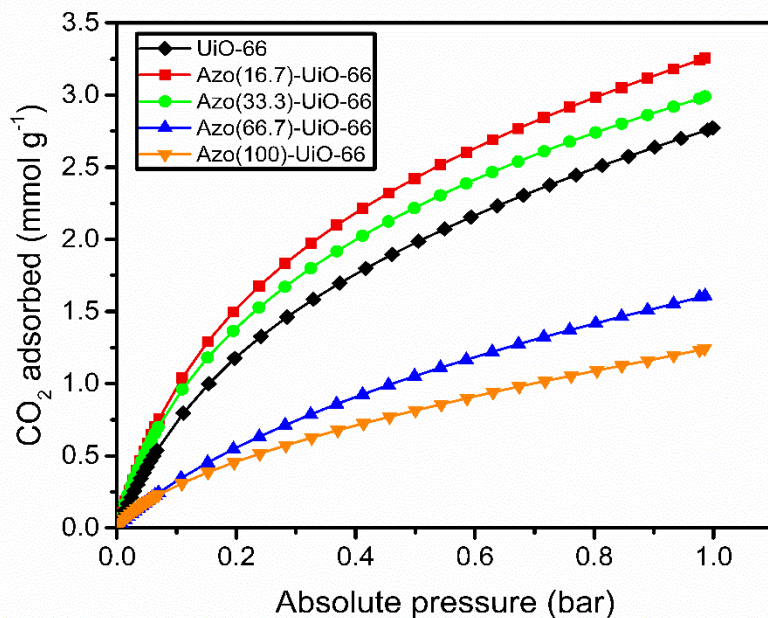


Figure S 12. CO₂ adsorption of UiO-66 and Azo(X)-UiO-66 at 273 K

The light-responsive property of the Azo(X)-UiO-66 MOFs were also evaluated at 273 K and the result is given in Figure S 13. It could be seen that the dynamic photoswitching property of the MOFs could also be maintained as also observed at 298 K. The trend of the percentage of CO₂ desorbed during UV light irradiation was also consistent with the ones observed at 298 K. Azo(16.7)-UiO-66 showed the lowest percentage of CO₂ desorbed during UV light irradiation and this value also reached plateau for both Azo(66.7)- and Azo(100)-UiO-66.

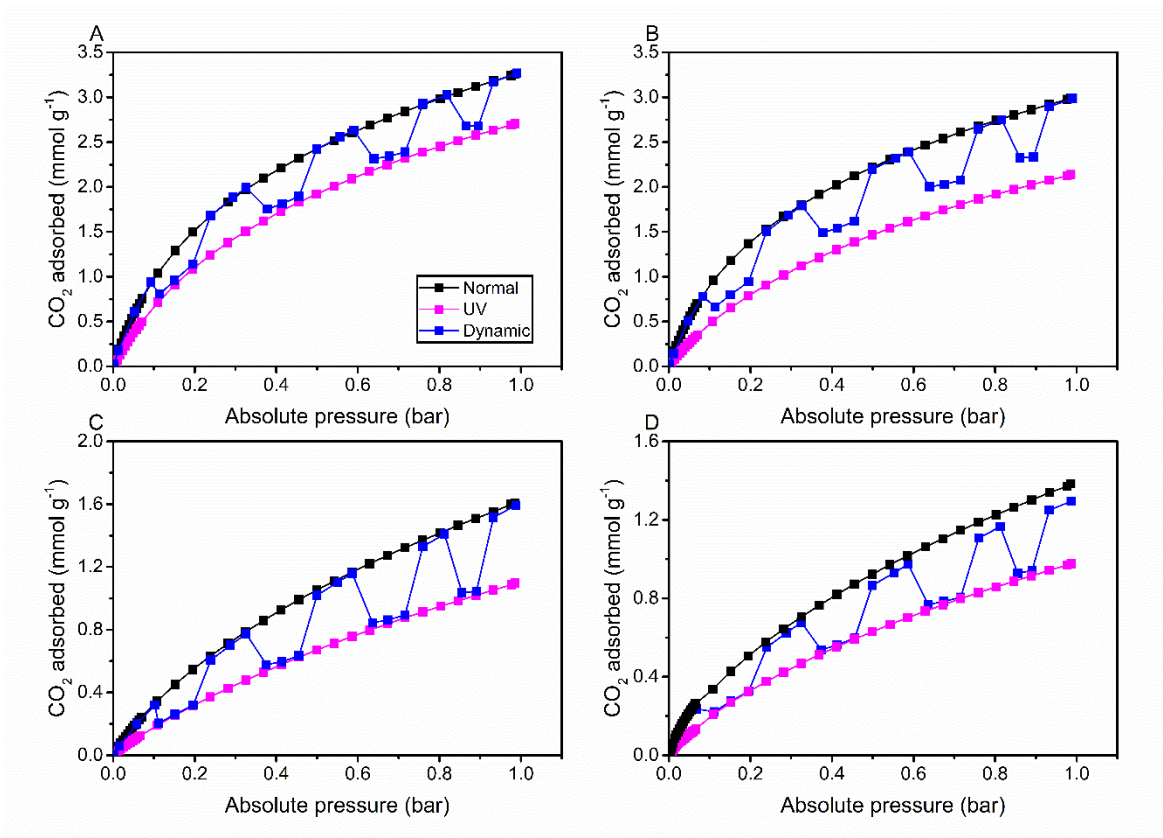


Figure S 13. CO₂ dynamic photoswitching of Azo(X)-UiO-66 at 273 K

MMMs characterizations

The PXRD diffraction patterns and FTIR spectra of all the MMMs are given in Figure S 14 and Figure S 15, respectively.

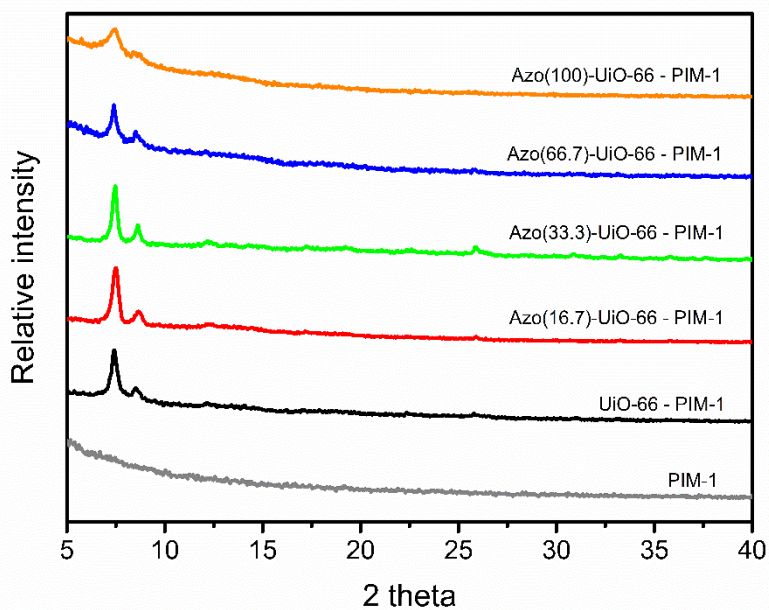


Figure S 14. PXRD diffraction pattern of the membranes

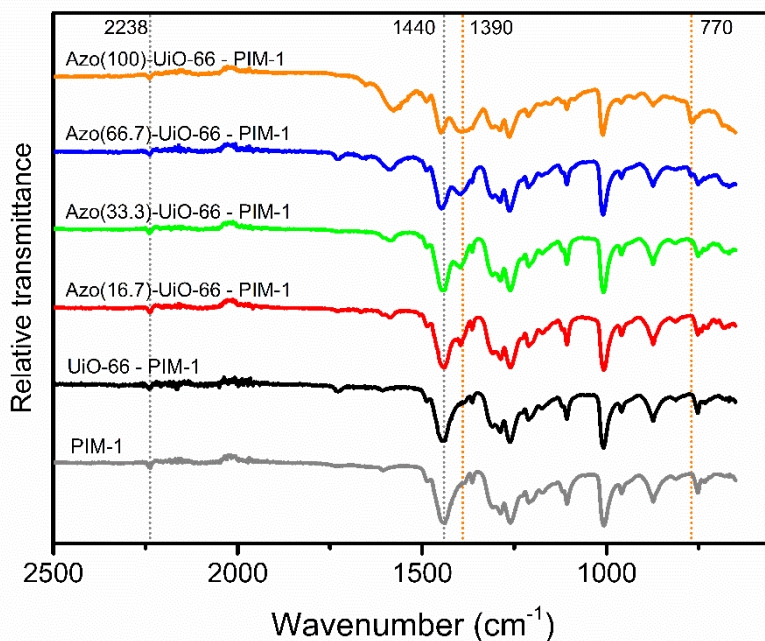


Figure S 15. FTIR spectra of the membranes

Additional micrographs of the cross-section of all the MMMs used in this study are given below showing the microstructure of the membrane and the particles that could be dispersed inside the matrix.

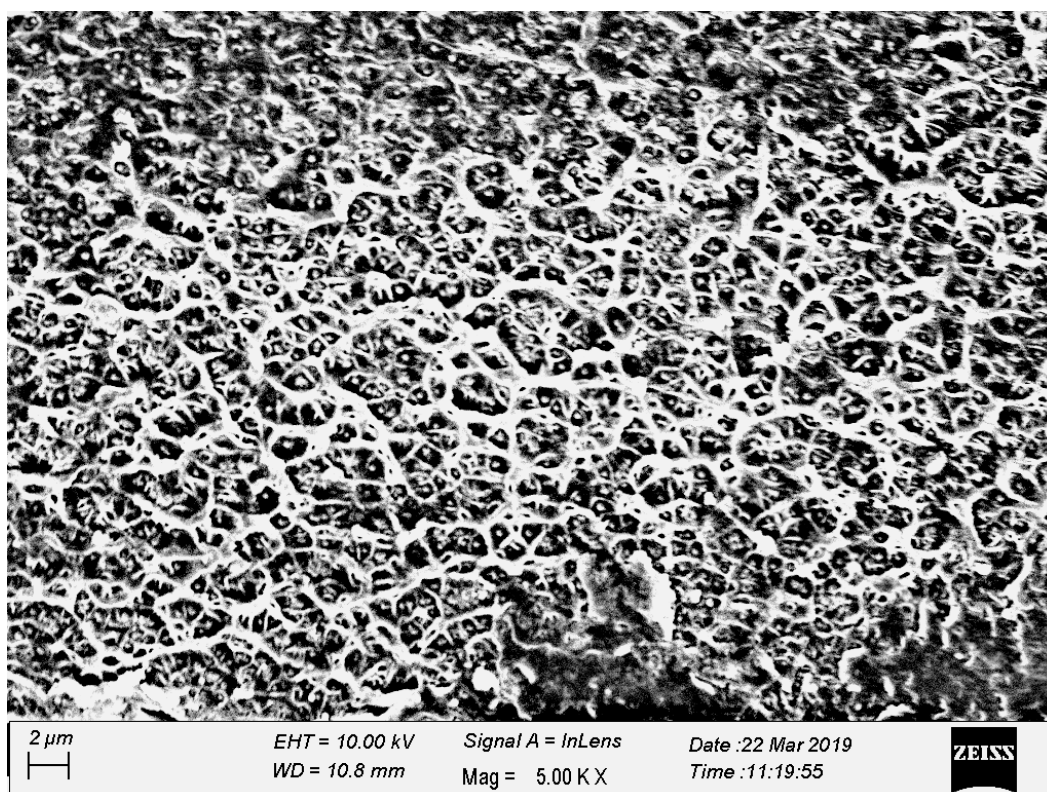


Figure S 16. SEM micrograph of UiO-66 – PIM-1 cross section

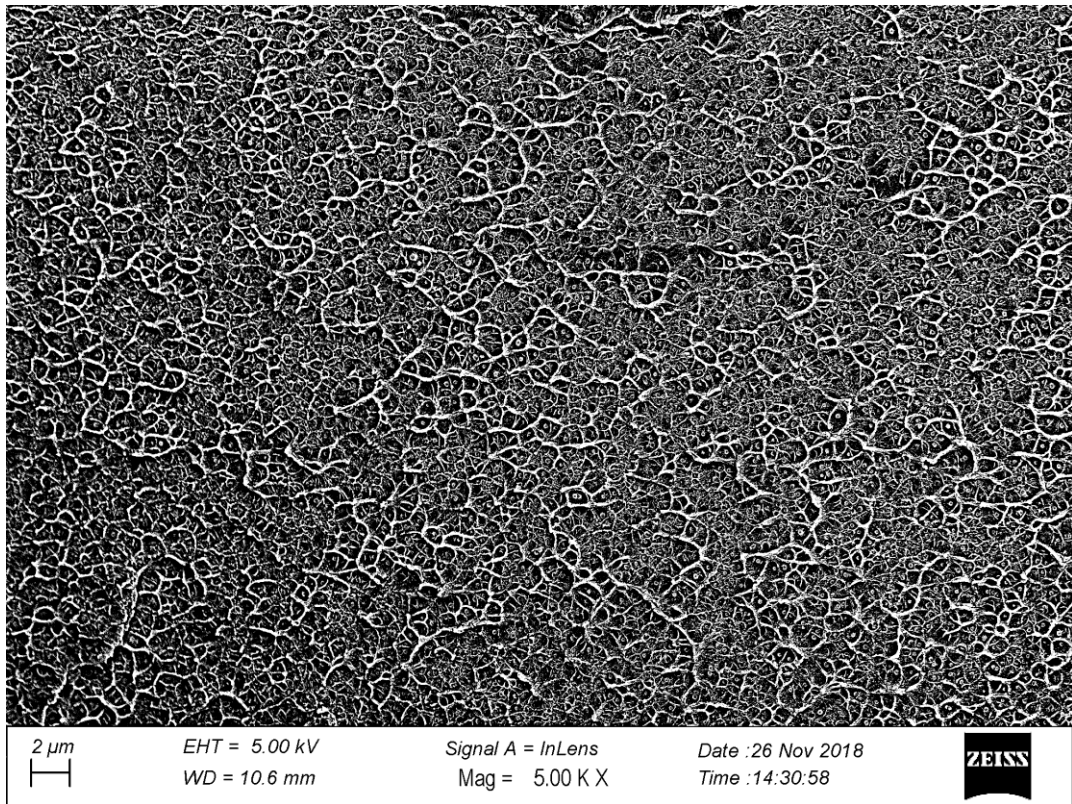


Figure S 17. SEM micrograph of Azo(16.7)-UiO-66 – PIM-1 cross section

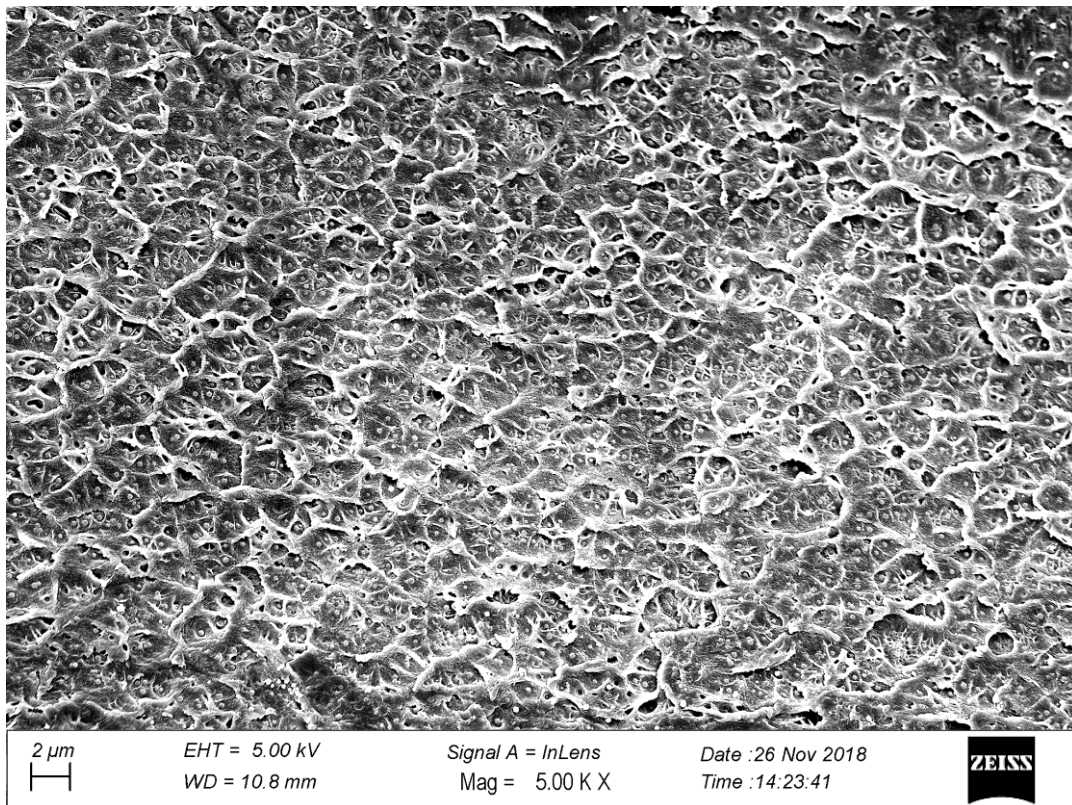


Figure S 18. SEM micrograph of Azo(33.3)-UiO-66 – PIM-1 cross section

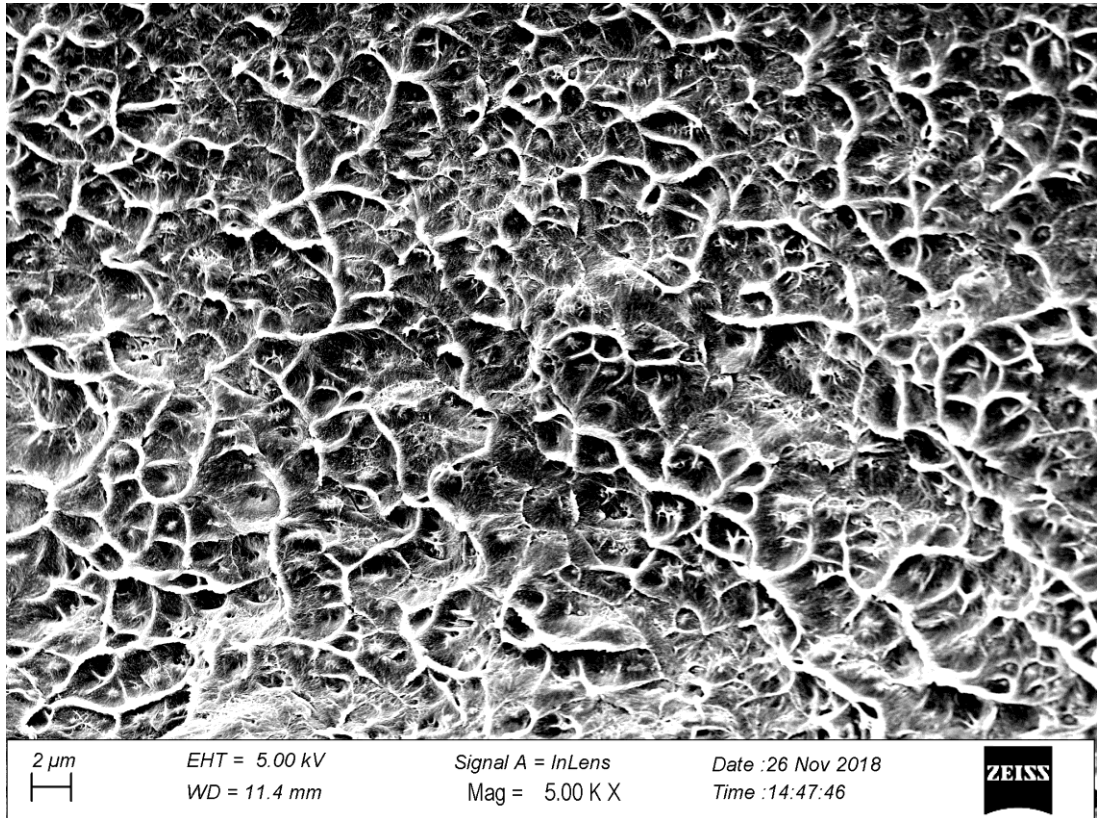


Figure S 19. SEM micrograph of Azo(66.7)-UiO-66 – PIM-1 cross section

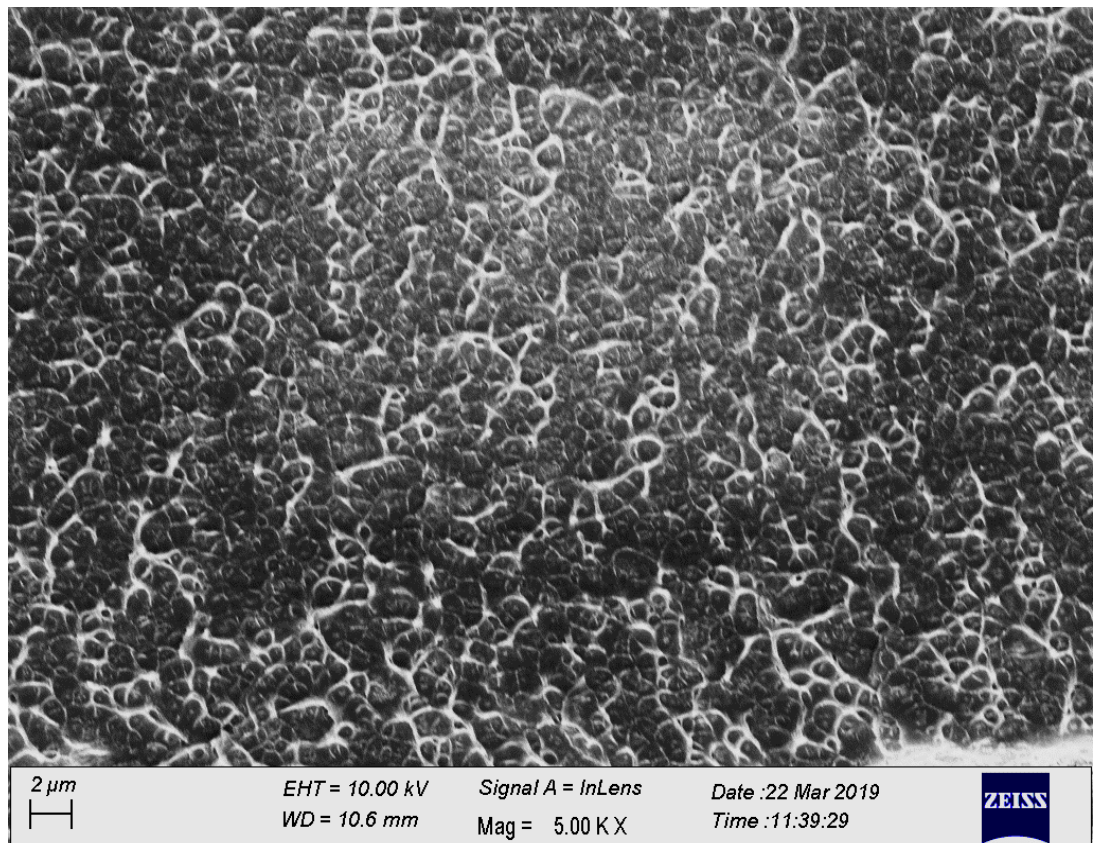


Figure S 20. SEM micrograph of Azo(100)-UiO-66 – PIM-1 cross section

The CO₂ adsorption of all the membranes at 298 K and up to 1 bar is given in Figure S 21. A similar trend was observed between the MOFs and MMMs. As can be seen, for UiO-66 – PIM-1, Azo(16.7)-UiO-66 – PIM-1 and Azo(33.3)-UiO-66 – PIM-1 had comparable CO₂ adsorption capacity with PIM-1. However, a decrease in CO₂ adsorption capacity could be observed for both Azo(66.7)-UiO-66 – PIM-1 and Azo(100)-UiO-66 – PIM-1. This is in line with the previous observation with the CO₂ adsorption of the MOFs where both MOFs had the lowest CO₂ adsorption capacity because of the significance occupation of the pores with azobenzene.

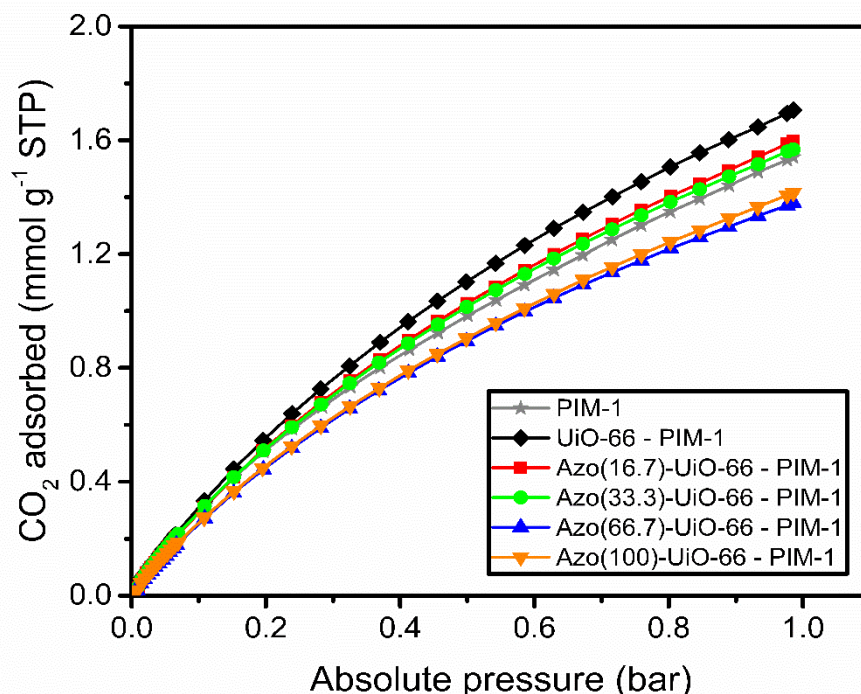


Figure S 21. CO₂ adsorption of the membranes used in this study

The N₂ adsorption of the all the membranes are given in Figure S 22. As with CO₂ adsorption, the lowest N₂ adsorption capacity of the MMMs were found in both Azo(66.7)-UiO-66 – PIM-1 and Azo(100)-UiO-66 – PIM-1. Their value was found to be significantly lower compared with the pristine PIM-1 and both UiO-66 – PIM-1 and Azo(16.7)-UiO-66 – PIM-1. Also, compared with the decrease in CO₂ uptake, the decrease in N₂ uptake for both Azo(66.7)-UiO-66 – PIM-1 and Azo(100)-UiO-66 – PIM-1 were more significant resulting in an increase in CO₂/N₂ adsorption ideal selectivity. This partially explains the increased CO₂/N₂ selectivity found in the membrane performance since it shows the decrease in N₂ affinity with the membranes loaded with MOFs that had higher azobenzene loading inside the framework.

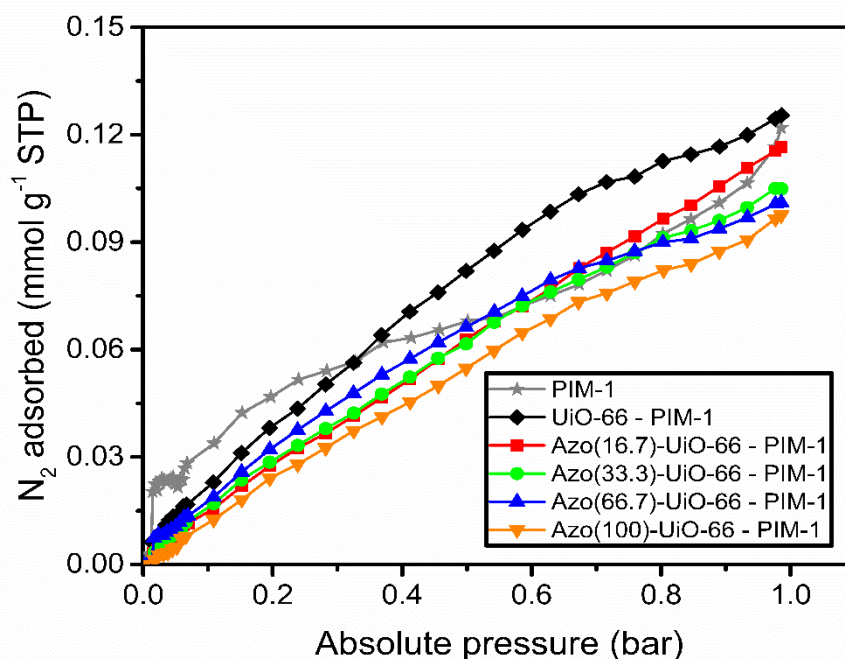


Figure S 22. N₂ adsorption of the membranes used in this study

Furthermore, these both data are also used to analyze the gas transport across the membranes. This was estimated in the scenario of 15:85 mixture of CO₂:N₂. The solubility coefficient value was calculated based on the previously described approach.^[4] In brief, the adsorption data in mmol g⁻¹ unit was converted to cm³ cm⁻³ cmHg⁻¹ by applying density. Afterwards, the diffusivity value was obtained from dividing the permeability value at 15:85 condition with the solubility value as in the equation below.

$$D_i = P_i/S_i$$

For N₂, the solubility coefficient value was obtained from the adsorption data point at 1 bar. Meanwhile, for the CO₂, the solubility coefficient was calculated based on the adsorption data point at 0.17 bar and thus resulting in total pressure of 1.17 bar. Although not exactly the same, this total pressure was close to the total pressure during the membrane operation around 1.3 bar and thus the calculation result should be reasonable to gain some insights on the gas transport properties.

Table S 3. Diffusivity and solubility coefficient of the membranes used in this study calculated from the adsorption data

Membrane	CO ₂		N ₂		S _{DCO₂/N₂}	S _{SCO₂/N₂}
	Diffusivity (x 10 ⁸ cm ² s ⁻¹)	Solubility (x 10 ² cm ³ cm ⁻³ cmHg ⁻¹)	Diffusivity (x 10 ⁸ cm ² s ⁻¹)	Solubility (x 10 ² cm ³ cm ⁻³ cmHg ⁻¹)		
PIM-1	83.9237	77.764	152.07	3.641	0.55188	21.35945
UiO-66 - PIM-1	121.281	83.815	216.225	3.745	0.5609	22.37875
Azo(16.7)-UiO-66 - PIM-1	112.986	78.536	198.211	3.48	0.57003	22.56926
Azo(33.3)-UiO-66 - PIM-1	110.022	78.327	200.025	3.133	0.55004	24.99821
Azo(66.7)-UiO-66 - PIM-1	129.533	68.091	205.12	3.019	0.6315	22.55704
Azo(100)-UiO-66 - PIM-1	137.12	69.01	189.911	2.913	0.72203	23.68627

Table S 4 gives a performance comparison of the membranes used in this study and PIM-1 based mixed matrix membranes.

Table S 4. PIM-1 based mixed matrix membranes CO₂/N₂ performance comparison

Filler	Filler loading (wt%)	Operating condition	Normalized CO ₂ permeability ^a	Ideal CO ₂ /N ₂ normalized selectivity ^a	
UiO-66-(COOH) ₂ ^[5]	16.6	1 bar; 298 K	1.1	0.9	
	28.6		1.2	0.8	
SNW-1 (COF) ^[6]	5	3.5 bar; 298 K	1.65	1.2	
	10		2.05	1.3	
	15		2.16	1.37	
ZIF-8 ^[7]	28	1 bar; 293-295 K	1.35	0.62	
	43		1.55	0.43	
	5		1.3	1.02	
NH ₂ -MIL-101(Cr) ^[8]	10	3 bar; 298 K	1.36	0.88	
	15		1.4	0.8	
UiO-66 ^[9]	5		1.35	1	
	10		1.4	1.01	
	20		1.5	0.8	
UiO-66-H ^[9]	5		1.7	1.42	
	10		1.64	1.46	
	20		1.6	1.52	
	30		0.66	1.13	
	40		0.32	1.33	
UiO-66-NH ₂ ^[9]	5	4 bar; 298 K	1.47	1.67	
	10		1.45	1.7	
	20		1.24	1.47	
	30		1.11	1.36	
	40		1.1	1.49	
UiO-66-Br ^[9]	5		1.62	1.24	
	10		1.25	1.34	
	20		0.87	1.19	
	30		0.8	1.18	
UiO-66 (this work)	10	20 psia; 298 K	0.76	1.46	
			Azo(16.7)-UiO-66(this work)	1.79	1
			Azo(33.3)-UiO-66 (this work)	1.63	1.11
Azo(66.7)-UiO-66 (this work)			1.51	1.1	
Azo(100)-UiO-66 (this work)			1.49	1.25	
			1.5	1.4	

^a this value is based on the reported pristine PIM-1 for each literature

3. Supplementary References

- [1] S. M. Chavan, G. C. Shearer, S. Svelle, U. Olsbye, F. Bonino, J. Ethiraj, K. P. Lillerud, S. Bordiga, *Inorg. Chem.* **2014**, 53, 9509.
- [2] X. Liu, N. K. Demir, Z. Wu, K. Li, *J. Am. Chem. Soc.* **2015**, 137, 6999.
- [3] N. Prasetya, B. C. Donose, B. P. Ladewig, *J. Mater. Chem. A* **2018**, 6, 16390.
- [4] A. Sabetghadam, X. Liu, M. Benzaqui, E. Gkaniatsou, A. Orsi, M. M. Lozinska, C. Sicard, T. Johnson, N. Steunou, P. A. Wright, *Chemistry—A European Journal* **2018**, 24, 7949.
- [5] M. R. Khdayyer, E. Esposito, A. Fuoco, M. Monteleone, L. Giorno, J. C. Jansen, M. P. Attfield, P. M. Budd, *Sep. Purif. Technol.* **2017**, 173, 304.
- [6] X. Wu, Z. Tian, S. Wang, D. Peng, L. Yang, Y. Wu, Q. Xin, H. Wu, Z. Jiang, *J Memb Sci.* **2017**, 528, 273.
- [7] A. F. Bushell, M. P. Attfield, C. R. Mason, P. M. Budd, Y. Yampolskii, L. Starannikova, A. Rebrov, F. Bazzarelli, P. Bernardo, J. C. Jansen, *J Memb Sci.* **2013**, 427, 48.
- [8] J. Ma, Y. Ying, X. Guo, H. Huang, D. Liu, C. Zhong, *J. Mater. Chem. A* **2016**, 4, 7281.
- [9] B. Ghalei, K. Sakurai, Y. Kinoshita, K. Wakimoto, A. P. Isfahani, Q. Song, K. Doitomi, S. Furukawa, H. Hirao, H. Kusuda, *Nat. Energy.* **2017**, 2, 17086.